An Undersampling Communication System Based on Compressive Sensing and In-Fiber Grating

Guoqing Wang , Dongrui Xiao , Li-Yang Shao, *Senior Member, IEEE*, Fang Zhao , Jie Hu, Shuaiqi Liu , Huanhuan Liu , Chao Wang , *Member, IEEE*, Rui Min , and Zhijun Yan

Abstract—An undersampling free-space optical (FSO) communication system based on compressive sensing (CS) and in-fiber grating is proposed. Our proposal drastically mitigates the data scale unfavorable issue and reduces the great amount of required data. Also, our proposal employs low-bandwidth and low-cost photodetectors (PDs) and analog-to-digital converters (ADCs) and decreases the cost of data detection. Besides, the data transmitted in the free space is encrypted, which enhances the security of the system. The in-fiber grating, which has the advantage of highly efficient thanks to its inherent compatibility with optical fiber links, plays the roles of light emitter, in-fiber polarizer, and light diffraction device, simultaneously. A sinusoidal radio frequency (RF) signal with a frequency of 1 GHz is utilized for a 2.4 m data transmission. And each PD with a bandwidth of 300 MHz is employed for detecting the transmitted signal on each channel. The proposal obtains data compression ratios of 25%, 15%, and 5% both in the temporal domain and frequency domain. Besides, a two-tone signal and a random RF signal are applied in the proposed FSO transmission for data transmission. Our proposal not only has the merits of secure, compact, stable, and highly efficient, but also has great potential in extremely secure situations, such as secured indoor and under water data communication.

Index Terms—Fiber gratings, diffractive optics, free-space communication, fiber optics systems, photodetectors.

Guoqing Wang, Dongrui Xiao, Fang Zhao, Jie Hu, Shuaiqi Liu, and Huanhuan Liu are with the Department of Electrical and Electronic Engineering, Southern University of Science and Technology, Shenzhen 518055, China (e-mail: wanggq@sustech.edu.cn; 11849550@mail.sustech.edu.cn; 12031197@mail.sustech.edu.cn; 12031313@mail.sustech.edu.cn; 11853004@mail.sustech.edu.cn; liuhh@sustech.edu.cn).

Li-Yang Shao is with the Department of Electrical and Electronic Engineering, Southern University of Science and Technology, Shenzhen 518055, China, and also with the Peng Cheng Laboratory, Shenzhen 518005, China (e-mail: shaoly@sustech.edu.cn).

Chao Wang is with the School of Engineering and Digital Arts, University of Kent, Canterbury CT2 7NT, U.K. (e-mail: c.wang@kent.ac.uk).

Rui Min is with the Center for Cognition and Neuroergonomics, State Key Laboratory of Cognitive Neuroscience and Learning, Beijing Normal University at Zhuhai, Zhuhai 519087, China (e-mail: ruimin@bnu.edu.cn).

Zhijun Yan is with the School of Optical and Electronic Information, Next Generation Internet Access National Engineering Laboratory, Huazhong University of Science and Technology, Wuhan 430074, China (e-mail: yanzhijun@hust.edu.cn).

Digital Object Identifier 10.1109/JPHOT.2021.3118699

I. INTRODUCTION

FREE-SPACE optical (FSO) communication attracts a great amount of attention in the past few decades due to its superiorities in security, anti-interception, insensitive to electromagnetic interference, good direction, and wide unlicensed band, which make it a promising and desirable candidate for future indoor and underwater communication applications [1]–[4]. Compared to the visible light FSO communication system, the infrared light FSO communication system not merely has the benefits of easy access, flexibility, and low-cost, but also takes the advantage of well-developed fiber devices and mature transmission technology [5]. In the infrared light FSO communication system, beam steering is always required to cover a wide range [1]–[3]. Normally, beam steering has active and passive solutions [6]. Previously, active beam steering has been implemented extensively thanks to its merits of low-cost and ease of manufacture. However, the drawbacks of low-speed and high-volume limit its application fields especially in the high-bandwidth communication area [7]. On the other hand, the passive beam steering has been successfully applied in wavelength tuning [8] and optical phased arrays [9] due to its benefits of compact size, high-speed, and mechanical free. However, the passive beam steering devices have high coupling loss with the fiber links.

Hence, one issue that existed in the FSO communication system is the requirement of a proper beam steering device candidate, which has to meet the needs of high-speed wavelength tuning, compact size, low-cost, and low coupling loss between the device candidate and the fiber links. And based on our previous work [2], [5], a compact and highly efficient in-fiber grating is utilized for the beam steering device. Another one is the data scale unfavourable issue: too much data to be detected and processed for the multiple high-bandwidth communication. Therefore, we present a method called compressive sensing (CS), which overcomes the Nyquist-Shannon sampling theorem. CS is a specific signal processing approach, which reconstructs the transmitted signal with high efficiency based on the proposition that the original signal is sparse in the transformation domain (e.g., spectral or temporal domain) [10]–[12]. The original sparse signal can be reconstructed from far fewer samples by optimization. The effort of implement CS has been successfully achieved in single-pixel imaging [13], digital signal processing [14], radio frequency (RF) signal measurement [15], laser scanning microscopy [16], optical coherence tomography (OCT) [17], [18], photonic time-stretch ADC [19], [20] and quantum communication [21].

To overcome the above limitations and based on our previous work [2], [5], we propose and experimentally demonstrate an

undersampling FSO communication system based on CS and in-fiber grating, which has the benefit of secure, compact, highly stable, and highly efficient. As a core device, the in-fiber grating, namely 45° tilted fiber grating (TFG), plays the roles of (a) a light emitter emitting light from fiber core into open free-space for data transmission, (b) a highly efficient and compact in-fiber polarizer ensuring the maximum efficiency of the system thanks to its polarization-sensitive characteristic, and (c) a light diffraction device obtaining wavelength-dependent lateral diffraction and providing a beam steering solution in our proposed system. Thanks to the utilization of CS, the transmitted data in the free-space and detected by the PD is encrypted resulting from the mixing of the RF signal and pseudo random binary sequences (PRBSs) in the temporal domain. Based on the theory of public-key cryptography, or asymmetric cryptography [22], the PRBSs perform as the public key, while the CS reconstruction algorithm and the setup of PRBSs (e.g., period or starting point) act as the private key. In comparison with the traditional FSO communication system, the data is encrypted before data transmission, which greatly enhances the security of the system. What's more, the employment of CS mitigates the data scale issue: much fewer data are detected by a low-bandwidth PD instead of an expensive high-bandwidth PD. As a result, low-cost and low-bandwidth PDs and followed-by ADCs can be utilized to deduce the cost of the FSO communication system. In addition, the employment of polarization modulation using a polarization modulator instead of intensity modulation using a Mach-Zehnder modulator (MZM) increases the stability of the proposed system based on our previous research [5]. A state-of-art demonstration is performed and a 1 GHz sinusoidal RF signal is detected by a 300 MHz PD after a free-space transmission of 2.4 m. Also, four channels with wavelengths of 1530 nm, 1540 nm, 1550 nm, and 1560 nm are used to certify the FSO communication. The experimental results show data compression ratios of 25%, 15%, and 5% both in the temporal domain and frequency domain. A two-tone signal is applied in our proposed FSO communication system and data compression ratios of 10% and 20% are obtained. Besides, a random RF signal with a maximum bandwidth of 300 MHz is employed for the FSO data transmission and data compression ratios of 15% and 20% are achieved. Our proposal greatly improves the stability and efficiency, and enhances the security of traditional FSO communication systems, and decreases the cost of the system by employing low-cost compact devices and low-bandwidth detectors and ADCs. This concept of undersampling FSO communication is extremely promising in many of great significance practical fields such as secured communication, indoor and under water data communication.

II. PRINCIPLE

TFGs mainly have three types: tilted fiber Bragg gratings, radiative TFGs, and excessive TFGs. The tilted fiber Bragg grating with a tilted angle (normally smaller than 10°) couples the light from propagating core mode into backward cladding mode, which is suitable for humidity and temperature sensing applications [23]. On the contrary, the excessive TFG couples light from propagating core mode into forward cladding mode, which is employed for index sensing [24]. In comparison with the tilted fiber Bragg gratings and excessive TFGs, the radiative TFG has a tilted angle range from 23.1° to 66.9° to the perpendicular axis of the propagation direction and it radiates
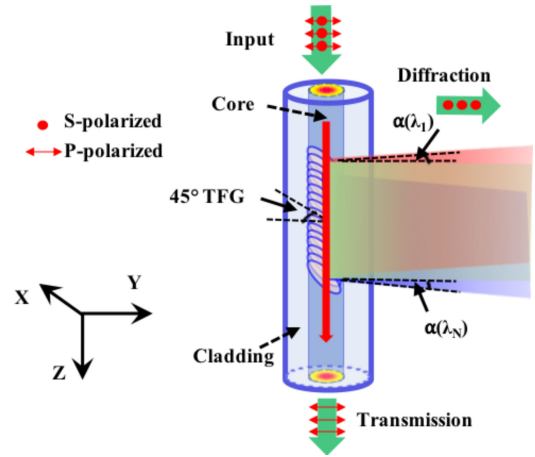

Fig. 1. Structure and working principle of 45° TFG, which shows its wavelength-dependent lateral diffraction and polarization-sensitive features. TFG: tilted fiber grating.

the incident light from fiber core into open space with strongly polarization-sensitive feature and wavelength-dependent lateral diffraction characteristic. The radiative TFG has been applied as an in-fiber polarizer [25], optical spectrum analyzer [26], and interrogator [27]. In particular, the 45° TFG is a special type of radiative TFGs, which has the maximum angular dispersion [28] and allows all the "S-polarized" light out of the fiber core for lateral diffraction and "P-polarized" light for transmission. Note, the "S-polarized" light and "P-polarized" light is not evenly distributed in the laser and the polarization state of the laser can be tuned by a polarization controller or a polarization modulator. In the previous research [28], the 45° TFG has been used as an in-fiber polarizer due to its highly polarization-sensitive characteristics and its polarization-dependent loss can be as high as 40 dB. Recently, the 45° TFG is reported as a compact, highly efficient in-fiber grating, which has been successfully applied in spectrally encoded imaging systems [29], time-stretch imaging systems [30], [31], mode-locked fiber lasers [32]–[34], and FSO communication systems [2], [5].

The structure and working principle of the 45° TFG are shown in Fig. 1, which depicts the wavelength-dependent lateral diffraction and polarization-sensitive features: the "S-polarized" incident light for lateral diffraction and the "P-polarized" incident light for transmission. Due to the asymmetric structure of 45° TFG, a strongly polarization-sensitive feature is obtained. In our experiment, a 45° TFG with a length of 24 mm and an angular dispersion of 0.0541°/nm is employed. Previously, a detailed theoretical analysis and experiment demonstration of 45° TFG has been reported [28]. Based on the previous analysis and according to the mode-coupling mechanism [28], the diffraction angle (α) of a radiative TFG in the free-space is defined as,

$$\sin \alpha = \frac{n \cdot \left(\cot \theta - \frac{n\Lambda}{\lambda \sin \theta} \right)}{\sqrt{1 + \left(\cot \theta - \frac{n\Lambda}{\lambda \sin \theta} \right)^2}} \qquad (1)$$

Where θ is the tilted angle of TFG, λ is the wavelength of the diffracted optical light, and n is the refractive index of the fiber core. Based on our previous theoretical and experimental analysis, the diffraction angle (α) has a linear relationship with the wavelength of incident optical light [14], which confirms the
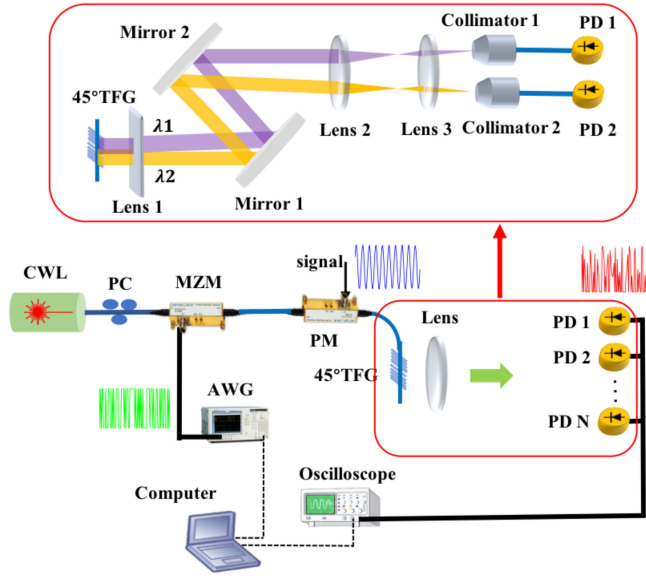
Fig. 2. Schematic of the proposed FSO communication system. FSO: free-space optical; CWL: continuous wavelength laser; PC: polarization controller; MZM: Mach-Zehnder modulator; AWG: arbitrary wavelength generator; PM: phase modulator; TFG: tilted fiber grating; PD: photo-detector.

Fig. 3. The propagating loss and insert loss in our proposed system at a transmission distance of 2.4 m.

wavelength-dependent lateral diffraction characteristics of the 45° TFG. The angular dispersion (D) of a 45° TFG is defined as the variation of wavelengths in corresponding to the differences of diffraction angles, which can be expressed as,

$$D = \frac{d\theta(\lambda)}{d\lambda} = -\frac{\text{nsin}(2\theta)}{\lambda} \tag{2}$$

And from equation (2), it's easy to get the conclusion that when the tilted angle (θ) of a radiative TFG is 45°, the angular dispersion has the maximum value for a certain wavelength and refractive index.

III. EXPERIMENTS AND RESULTS

The schematic of the proposed undersampling FSO communication system is shown in Fig. 2. A continuous wavelength laser (CWL) with an average optical power of 6 dBm is employed as the laser source. Light from CWL passes the polarization controller (PC), where the linear polarization state of the incident light is controlled. Then the light goes through the MZM, where the light is modulated by the pseudo random binary sequences (PRBSs) from an arbitrary waveform generator (AWG). The PRBSs from an AWG are sent to the computer simultaneously for the final data processing. The PRBS-modulated light propagates the phase modulator (PM) where a sinusoidal RF signal with a central frequency of 1 GHz is employed to modulate the light. Here the combination of PM and 45° TFG are applied for intensity modulation[35], [36]. The modulated light then reaches the 45° TFG and diffracts into free-space for a 2.4 m free-space data transmission. Here, the 45° TFG has three functions: (a) it emits the light from fiber core into open space for FSO data transmission due to its radiative feature of lateral diffraction, (b) it realizes polarization modulation and control as an in-fiber polarizer as well as obtains the maximum data and energy efficiency thanks to its polarization-sensitive characteristics, and (c) it achieves the point-to-point privacy channel communication
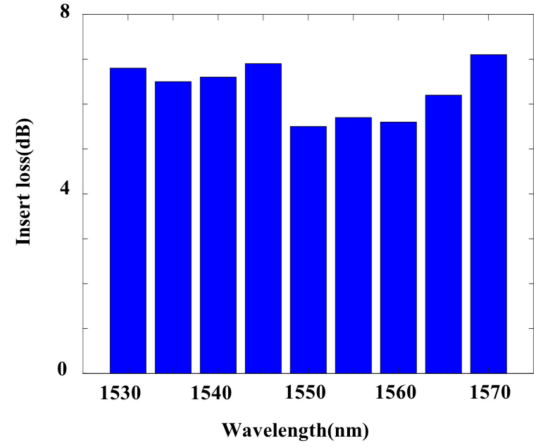
due to its wavelength-dependent feature of lateral diffraction as an in-fiber grating. What's more, based on our previous report [5], the utilization of PM and 45° TFG could drastically increase the system stability with the advantages of preventing the fluctuation of the intensity of the modulated signals.

The details of light transmission in the free-space are shown in the red square of Fig. 2. The modulated light emitted out of 45° TFG propagates a cylindrical lens with a focal length of 20 mm, which is employed to collimate the FSO light in the vertical direction. In our experiment, a pair of silver-coated mirrors changes the direction of light and expands the light propagating length, which is 2.4 m in our experiment. A telescope, consists of a pair of plano-convex lenses with focal lengths of 100 mm and 25 mm and separated by 125 mm, is employed to shrink the beam size for light reception. Then the wavelength-dependent free-space light reaches single-mode fiber collimators, which have a numerical aperture of 0.49. And several PDs with a bandwidth of 300 MHz receive the light from the collimators. An oscilloscope with a tunable bandwidth and sampling rate is utilized to illustrate the detected waveforms. Finally, the waveform data from the oscilloscope and the PRBSs data from AWG are employed to recover the RF signal thanks to the CS algorithm.

The high-efficiency advantage of 45° TFG is confirmed by measuring its point-to-point propagating and insert loss at a wavelength range from 1530 nm to 1570 nm with a step of 5 nm. The point-to-point propagating loss and insert loss in our undersampling FSO communication system is defined as the power difference of the incident light to the 45° TFG and the light received by the PD. Fig. 3 shows the propagating loss and insert loss, which has a variation of from 5.3 dB to 7.1 dB at a wavelength range from 1530 nm to 1570 nm at a free-space transmission distance of 2.4 m. The result confirms that 45° TFG is a highly efficient in-fiber compact device, which has neglectable propagating loss within a short distance and is suitable for indoor FSO communication system.

Four optical carriers with wavelengths of 1530 nm, 1540 nm, 1550 nm, and 1560 nm are used to serve four remote users in our proposed system. The remote users receive the data after a working distance of 2.4 m. A low-cost PD with a bandwidth of 300 MHz is utilized to receive the data at each user site. A privacy point-to-point data transmission is obtained owing to
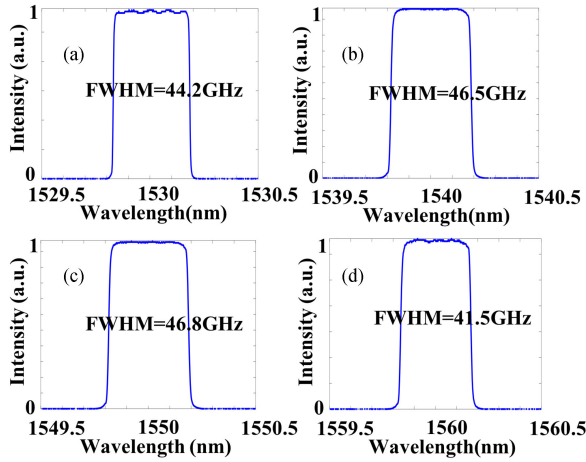
Fig. 4. Spectral response for four users with optical carrier wavelengths of (a) 1530, (b) 1540, (c) 1550, and (d) 1560 nm, and the full width at half maximum (FWHM) of which are 44.2 GHz, 46.5 GHz, 46.8 GHz, and 41.5 GHz, respectively.
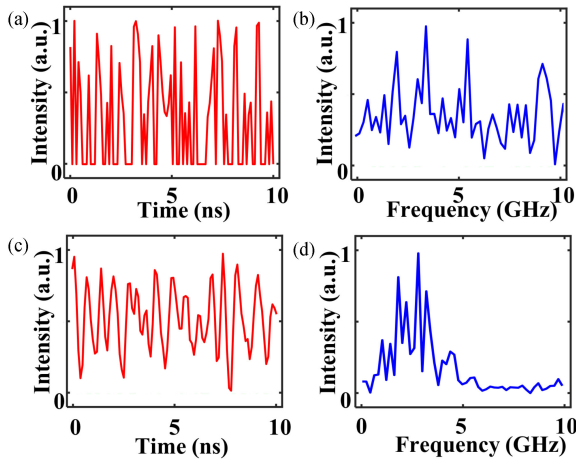

Fig. 5. (a) The direct detected data by a PD with a bandwidth of 10 GHz; (b) Fast Fourier transformation of (a); (c) the direct detected data by a PD with a bandwidth of 300 MHz; (d) Fast Fourier transformation of (c).

the wavelength-dependent feature of the 45° TFG. The spectral response of four users with wavelengths of 1530 nm, 1540 nm, 1550 nm, and 1560 nm (shown in Fig. 4) are measured at varied physical positions, and the full width at half maximum (FWHM) of which are 44.2 GHz, 46.5 GHz, 46.8 GHz, and 41.5 GHz, respectively. The differences in FWHM of varied wavelengths are mainly induced by optical coupling from free-space to single-mode fiber via the collimator. In Fig. 4, the wide bandwidths provide the potential of high-speed FSO data transmission in our proposed system. Besides, the measured spectral bandwidth is flat, which allows optical carrier wavelength drift at a reasonable scope and permits a certain range of physical position movement.

To confirm our proposed undersampling FSO communication system, a fast PD with a bandwidth of 10 GHz is employed in comparison with the above 300 MHz PD. The direct detected data, which is the mixing of 1 GHz sinusoidal RF signal and PRBSs, is received by the fast 10 GHz PD followed by an oscilloscope with a bandwidth of 4 GHz. Fig. 5(a) describes the temporal waveform detected by the fast 10 GHz PD. In Fig. 5(a), the 1 GHz RF signal and PRBSs are fully mixed, and it's not

possible to reconstruct the RF signal only from the temporal waveform. Fig. 5(b) illustrates the mixed signal in the frequency domain by the fast Fourier transformation (FFT) of Fig. 5(a). Fig. 5(b) in the frequency domain confirms the inconsistency of RF signal and the mixed signal. The signal direct detected situation is repeated by using a 300 MHz PD. Fig. 5(c) depicts the temporal waveform of direct detection using a PD with a bandwidth of 300 MHz. It's easy to conclude that the 1 GHz RF signal and the mixed signal have obvious differences. The FFT of Fig. 5(c) is shown in Fig. 5(d), which is the waveform of mixed signal in the frequency domain. From Fig. 5, whether using a high bandwidth PD or a low bandwidth PD, the RF signal could not get reconstructed from the mixed signals whether in the temporal or frequency domain. This demonstration confirms our proposed system has the advantage of secure communication. Based on the asymmetric key encryption scheme, in our experimental setup, the PRBSs perform as the public key, and the CS reconstruct algorithm and the setup of PRBSs act as the private key. Only by combining the public and private keys, the exact RF signal can be reconstructed.

In our experiment for the CS algorithm setup, suppose the 1D sinusoidal signal $I_{M \times 1}$ has a length of M points. And it's mixed with N PRBSs that from the AWG, N is the number of measurements (N < M) and each measurement has the same length as $I_{M \times 1}$, which is M points. $I_{M \times 1}$ is defined as

$$I_{M \times 1} = \varphi_{M \times M} \times S_{M \times 1} \tag{3}$$

where $\varphi_{M \times M}$ is the Fourier orthogonal basis, and it has a size of M×M; $S_{M \times 1}$ is the transformation domain of $I_{M \times 1}$, and it has a size of M×1. The 1D sinusoidal signal has to obey the condition of sparsity in discreet Fourier transformation (DFT) domain. The measurement matrix $R_{N \times M}$ stands for N times of measurement with corresponding lengths of PRBSs (each PRBS has M points). Then the measurement vector $y_{N \times 1}$ with N times of measurement is expressed as

$$y_{N \times 1} = R_{N \times M} \times I_{M \times 1} = R_{N \times M} \times \varphi_{M \times M} \times S_{M \times 1}$$
$$= \theta_{N \times M} \times S_{M \times 1} \tag{4}$$

where $\theta_{N \times M} = R_{N \times M} \times \varphi_{M \times M}$, stands for the matrix product, and it has a size of N×M, and it has to meet the restricted isometry property [37].

The signal recovery process based on convex optimization is the process of reconstructing $I_{M \times 1}$ from $y_{N \times 1}$. The measurement vector $y_{N \times 1}$ is the measured data acquired from PD directly, and the measurement matrix $R_{N \times M}$ (the PRBSs matrix from AWG) is known. The matrixes $y_{N \times 1}$ and $R_{N \times M}$ are the input in our proposal. Hence, optimization of $S_{M \times 1}$ can be achieved with the utilization of total variation (TV) minimization algorithm using minimum l_1 norm reconstruction [38],

$$s = \arg \min(TV_1) \text{ subject to } \theta s = y \tag{5}$$

As a result, the introduction of transformation domain S is recovered. Furthermore, due to $I_{M \times 1} = \varphi_{M \times M} \times S_{M \times 1}$, the 1D sinusoidal signal information is finally reconstructed.

To confirm our proposed undersampling FSO communication system, which is described in Fig. 2, a proof-of-principle experiment is demonstrated. A sinusoidal signal with a frequency of 1 GHz serves as the original RF signal. Four optical carriers with wavelengths of 1530 nm, 1540 nm, 1550 nm, and 1560 nm standing for varied physical positions are used to serve as the
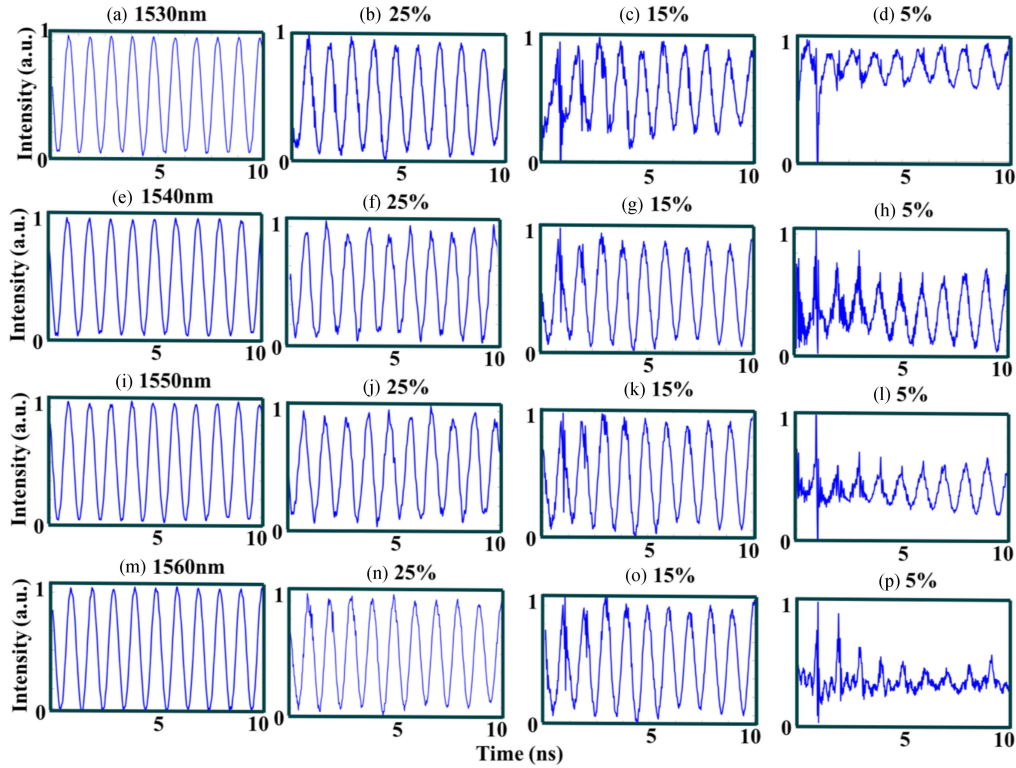
Fig. 6. The original signals [(a), (e), (i) and (m)] and recovered sinusoidal signals at varied compress ratios of 25% [(b), (f), (j) and (n)], 15% [(c), (g), (k) and (o)] and 5% [(d), (h), (l) and (p)] in the temporal domain at optical carrier wavelengths of (a) 1530 nm, (e) 1540 nm, (i) 1550 nm, and (m) 1560 nm, respectively.

four remote users. Each wavelength represents a point-to-point privacy channel. And the undersampling FSO communication system is obtained by the utilization of CS setup. In our CS configuration, M equals 400, which means the sinusoidal RF signal has 400 points; N is varied at 100, 60, and 20, which means 100, 60, and 20 times of measurements; y is the measured result from the 300 MHz PD and each measurement generates one data. Based on the above CS algorithm and minimum l_1 norm reconstruction, the reconstructed signal with data compression ratios of 25%, 15%, and 5% are achieved at the four optical carriers, respectively. Fig. 6 illustrates the original and reconstructed sinusoidal signals with a frequency of 1 GHz in the temporal domain at the optical carrier wavelengths of (a-d) 1530 nm, (e-h) 1540 nm, (i-l) 1550 nm, and (m-p) 1560 nm, respectively. In Fig. 6, (a), (e), (i), and (m) stand for the original input sinusoidal signals in the temporal domain, and (b-d), (f-h), (j-l), and (n-p) are the experimental results of reconstructed sinusoidal signals in the temporal domain with data compression ratios of 25%, 15%, and 5%, respectively. The results in Fig. 6 indicate that with a certain range of data compression ratios, such as from 25% to 15%, the reconstructed signals have good consistency with the original signals at the measured varied wavelengths. And with a 5% data compression ratio, the reconstructed signals still can be distinguished. Fig. 7 shows the original and reconstructed signals at the above four wavelengths in the spectral domain with data compression ratios of 25%, 15%, and 5%, respectively. In Fig. 7(a), (e), (i), and (m) are the original signals in the spectral domain, and (b-d), (f-h), (j-l), and (n-p) are the experimental results of reconstructed sinusoidal signals in the spectral domain with data compression ratios of 25%, 15%, and 5%, respectively. From Fig. 7, the reconstructed results indicate that the recovered

signals with different compression ratios and original signals are in good consistency in the spectral domain at varied wavelengths. The results from Figs. 5, 6, and 7, certify that our achievable and promising compact undersampling FSO communication system is secure and data-efficiency.

To confirm our FSO communication system is suitable for multiple frequencies. A two-tone signal on the optical carrier wavelength of 1550 nm is employed for the FSO transmission. However, due to the lack of a fast signal generator, a two-tone signal with the frequency of 10 MHz and 25 MHz is applied for the two-tone signal transmission. Fig. 8 describes the original two-tone signal and its reconstruction with data compression ratios of 10% and 20% in the temporal and the spectral domain. The original two-tone signal in the temporal domain and spectral domain is shown in Fig. 8(a) (blue line) and Fig. 8(b) (blue line), respectively. The red lines in Figs. 8(a) and 8(b) are the reconstructed results with a data compression ratio of 10%. The red lines in Figs. 8(c) and (d) show the reconstructed results with a data compression ratio of 20%. From Fig. 8, the original blue lines and reconstructed red lines show good consistency both in the temporal and spectral domain. Moreover, a further FSO transmission demonstration using a random RF signal on the optical carrier wavelength of 1550 nm is performed. The random RF signal has a maximum bandwidth of 300 MHz. Fig. 9 illustrates the original random RF signal and its reconstruction with data compression ratios of 15% and 20% in the temporal domain. The original random RF signal is shown in Fig. 9a (blue line). The red lines in Fig. 9 are the reconstructed results for the random RF signal with data compression ratios of 15% (a) and 20% (b). Fig. 9 indicates that the reconstructed results (red lines) are consistent with the original signal (blue lines). The
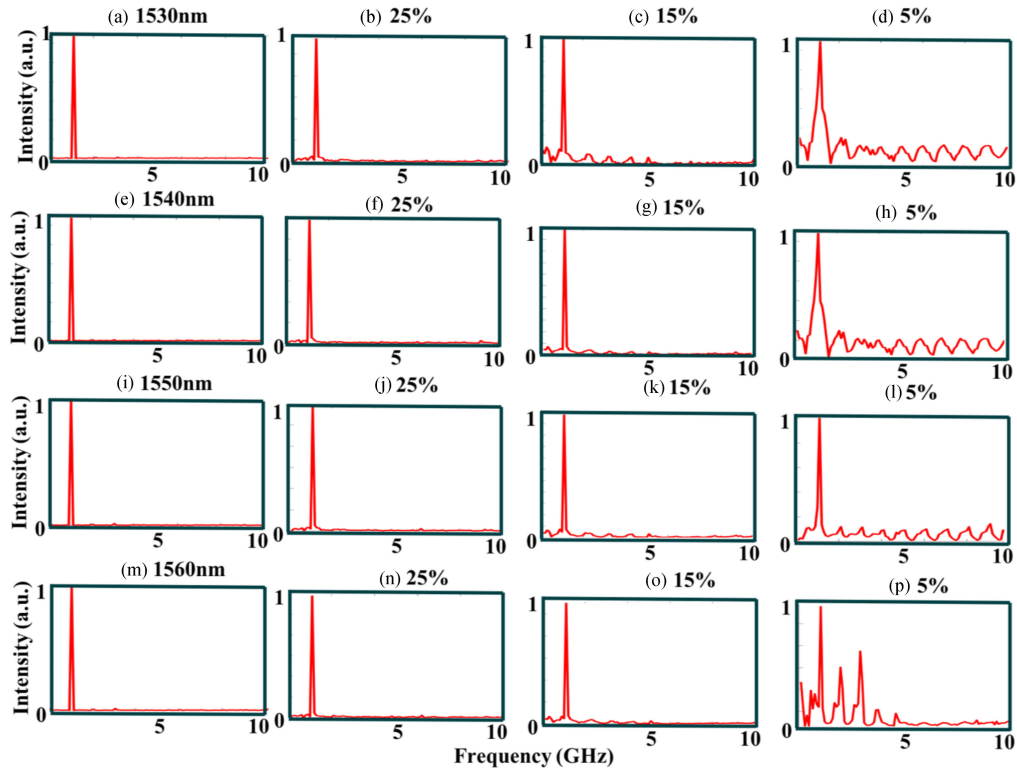
Fig. 7. The original signals [(a), (e), (i) and (m)] and recovered sinusoidal signals at compress ratios of 25% [(b), (f), (j) and (n)], 15% [(c), (g), (k) and (o)] and 5% [(d), (h), (l) and (p)] in the spectral domain at optical carrier wavelengths of (a) 1530 nm, (e) 1540 nm, (i) 1550 nm, and (m) 1560 nm, respectively.
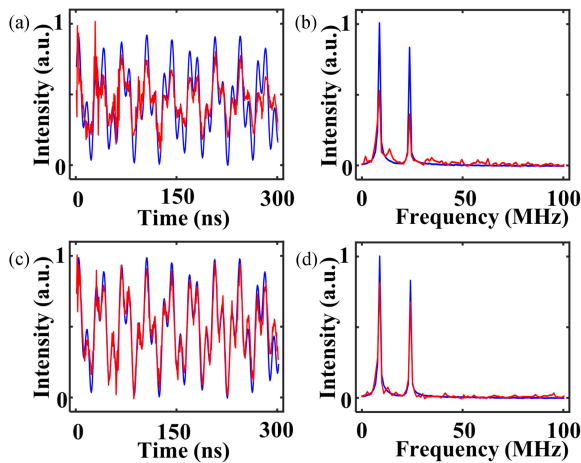

Fig. 8. The original two-tone signal (blue lines) and its reconstruction (red lines) with data compression ratios of 10% [(a), (b)] and 20% [(c), (d)] in the temporal domain and spectral domain.
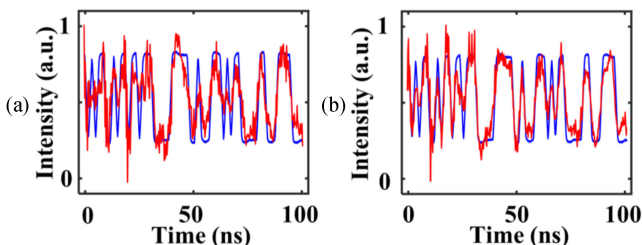

Fig. 9. The input RF signal (blue lines) and its reconstruction (red lines) with data compression ratios of 15% (a) and 20% (b) in the temporal domain.

CS process time in software is around 100ms, which could be ignored in the desired indoor and under water data communication application. Note our demonstration is performed in 1D, to perform a 2D demonstration as the future work, the combination of a virtually imaged phased array (VIPA) [39] and a diffraction in-fiber grating can be applied.

IV. CONCLUSION

In summary, we proposed and experimentally demonstrated a compact and highly efficient undersampling FSO communication system based on CS and in-fiber grating for the first time. The in-fiber grating, namely 45° TFG, has the benefits of high-efficiency, compact, and low insert loss thanks to its feature of compatibility with fiber links. The 45° TFG plays the roles of (a) lateral light emitter due to its radiative structure, (b) high-efficiency in-fiber polarizer resulting from its polarization-sensitive characteristics and realizing polarization modulation and control, and (c) in-fiber diffraction grating due to its wavelength-dependent lateral diffraction feature ensuring a point-to-point privacy channel for data transmission. A 2.4 m FSO data transmission is performed using a sinusoidal RF signal with a frequency of 1 GHz. And a PD with a bandwidth of 300 MHz is employed to detect the final transmitted signal. Four optical carriers with wavelengths of 1530 nm, 1540 nm, 1550 nm, and 1560 nm are used to serve as the remote four users. The experimental results in our proposed system show compression ratios of 25%, 15%, and 5%, respectively. And the reconstructed signals and the original signals have good consistency both in the temporal domain and spectral domain. Besides, a two-tone signal is applied in our proposed FSO

communication system and data compression ratios of 10% and 20% are obtained. Moreover, a random RF signal with a maximum bandwidth of 300 MHz is employed for the FSO data transmission and data compression ratios of 15% and 20% are achieved. The reconstructed two-tone signal and random RF signal and their original signals both show great consistency whether in the temporal domain or the spectral domain. The utilization of CS setup in our proposed system not only mitigates the data scale-unfavorable issue but also reduces the detection cost by using low-cost and low-bandwidth PDs and ADCs. As a result, our proposal paves the way for solving the energy and data efficiency bottleneck in the traditional FSO communication system. What's more, the data transmitted in the free space is encrypted thanks to the employment of CS. Hence, the security of the proposed system is greatly enhanced. The presented proposal has the benefits of secure, compact, stable, energy-efficiency, and data-efficient, which is extremely promising in secured indoor and under water data communication.

REFERENCES

[1] G. Wang *et al.*, "Highly efficient optical beam steering using an in-fiber diffraction grating for full duplex indoor optical wireless communication," *J. Lightw. Technol.*, vol. 36, no. 19, pp. 4618–4625, Oct. 2018.

[2] G. Wang, U. Habib, C. Wang, N. J. Gomes, Z. Yan, and L. Zhang, "Wavelength-controlled beam steering for optical wireless transmission using an in-fiber diffraction grating," in *Proc. Conf. Lasers Electro-Opt.*, San Jose, CA, USA, 2017, Art. no. SF1L.5.

[3] C. W. Oh, Z. Cao, E. Tangdiongga, and T. Koonen, "Free-space transmission with passive 2D beam steering for multi-gigabit-per-second per-beam indoor optical wireless networks," *Opt. Exp.*, vol.vol. 24, no.no. 17, pp. 19211–19227, 2016.

[4] K. Wang, A. Nirmalathas, C. Lim, and E. Skafidas, "High-speed duplex optical wireless communication system for indoor personal area networks," *Opt. Exp.*, vol. 18, no. 24, pp. 25199–25216, 2010.

[5] G. Wang *et al.*, "Stable and highly efficient free-space optical wireless communication system based on polarization modulation and in-fiber diffraction," *J. Lightw. Technol.*, vol. 39, no. 1, pp. 83–90, Jan. 2021.

[6] C. W. Oh, E. Tangdiongga, and A. M. J. Koonen, "Steerable pencil beams formulti-Gbps indoor optical wireless communication," *Opt. Lett.*, vol. 39, no. 18, pp. 5427–5430, 2014.

[7] A. Gomez *et al.*, "Beyond 100 Gb/s indoor wide field-of-view optical wireless communications," *IEEE Photon. Technol. Lett.*, vol. 27, no. 4, pp. 367–370, Feb. 2015.

[8] T. Chan, E. Myslivets, and J. E. Ford, "2-Dimensional beam steering using dispersive deflectors and wavelength tuning," *Opt. Exp.*, vol. 16, no. 18, pp. 14617–14628, 2008.

[9] J. K. Doylend, M. J. R. Heck, J. T. Bovington, J. D. Peters, L. A. Coldren, and J. E. Bowers, "Two-dimensional free-space beam steering with an optical phased array on silicon-on-insulator," *Opt. Exp.*, vol. 19, no. 22, pp. 21595–21604, 2011.

[10] C. Lei, B. Guo, Z. Cheng, and K. Goda, "Optical time-stretch imaging: Principles and applications," *Appl. Phys. Rev.*, vol. 3, 2016, Art. no. 011102.

[11] B. T. Bosworth, J. R. Stroud, D. N. Tran, T. D. Tran, S. Chin, and M. A. Foster, "High-speed flow microscopy using compressed sensing with ultrafast laser pulses," *Opt. Exp.*, vol. 2, no. 8, pp. 10521–10532, 2015.

[12] Q. Guo, H. Chen, Z. Weng, M. Chen, S. Yang, and S. Xie, "Compressive sensing based high-speed time-stretch optical microscopy for two-dimensional image acquisition," *Opt. Exp.*, vol. 23, no. 23, pp. 29639–29646, 2015.

[13] J. Shin, B. T. Bosworth, and M. A. Foster, "Single-pixel imaging using compressed sensing and wavelength-dependent scattering," *Opt. Lett.*, vol. 41, no. 5, pp. 886–889, 2016.

[14] B. Jalali and M. H. Asghari, "The anamorphic stretch transform: Putting the squeeze on 'Big data,'" *Opt. Photon. News*, vol. 25, no. 2, pp. 24–31, 2014.

[15] G. C. Valley, G. A. Sefler, and T. J. Shaw, "Compressive sensing of sparse radio frequency signals using optical mixing," *Opt. Lett.*, vol. 37, no. 22, pp. 4675–4677, 2012.

[16] N. Pavillon and N. I. Smith, "Compressed sensing laser scanning microscopy," *Opt. Exp.*, vol. 24, no. 26, pp. 30038–30052, 2016.

[17] C. K. Mididoddi, F. Bai, G. Wang, C. Liu, S. Gibson, and C. Wang, "High-Throughput photonic time-stretch optical coherence tomography with data compression," *IEEE Photon. J.*, vol. 9, no. 4, Aug. 2017, Art. no. 3901015.

[18] C. K. Mididoddi, G. Wang, and C. Wang, "Data compressed photonic time-stretch optical coherence tomography," in *Proc. IEEE Photon. Conf.*, Waikoloa, HI, USA, 2016, pp. 13–14.

[19] H. Chi, Y. Chen, Y. Mei, X. Jin, S. Zheng, and X. Zhang, "Microwave spectrum sensing based on photonic time stretch and compressive sampling," *Opt. Lett.*, vol. 38, no. 2, pp. 136–138, 2013.

[20] T. P. McKenna, J. H. Kalkavage, M. D. Sharp, and T. R. Clark, "Wideband photonic compressive sampling system," *J. Lightw. Technol.*, vol. 34, no. 11, pp. 2848–2855, Jun. 2016.

[21] C. A. Riofrio *et al.*, "Experimental quantum compressed sesing for a seven-qubit system," *Nature Commun.*, vol. 8, 2017, Art. no. 15305.

[22] H. Wu, F. Zhou, Z. Zhu, and Y. Chen, "Analysis framework of RSA algorithms in elastic optical rings," *J. Lightw. Technol.*, vol. 37, no. 4, pp. 1113–1122, 2019.

[23] J. Albert, L. Y. Shao, and C. Caucheteur, "Tilted fiber Bragg gratings sensors," *Laser Photon. Rev.*, vol. 7, no. 1, pp. 83–108, 2012.

[24] K. Zhou, L. Zhang, X. Chen, and I. Bennion, "Optic sensors of high refractive-index responsivity and low thermal cross sensitivity that use fiber Bragg gratings of >80° tilted structures," *Opt. Lett.*, vol. 31, no. 9, pp. 1193–1195, 2006.

[25] P. S. Westbrook, T. A. Strasser, and T. Erdogan, "In-line polarimeter using blazed fiber gratings," *IEEE Photon. Technol. Lett.*, vol. 12, no. 10, pp. 1352–1354, Oct. 2000.

[26] P. Cheben *et al.*, "Tilted fiber Bragg grating sensor interrogation system using a high-resolution silicon-on-insulator arrayed waveguide grating," *Opt. Lett.*, vol. 33, no. 22, pp. 2647–2650, 2008.

[27] S. Bandyopadhyay *et al.*, "Highly efficient free-space fiber coupler with 45 tilted fiber grating to access remotely placed optical fiber sensors," *Opt. Exp.*, vol. 28, no. 11, pp. 16569–16578, 2020.

[28] Q. He *et al.*, "In-fiber single-polarization diffraction grating based on radiant tilted fiber grating," *Opt. Lett.*, vol. 44, no. 17, pp. 4407–4410, 2019.

[29] G. Wang, C. Wang, Z. Yan, and L. Zhang. "Highly efficient spectrally encoded imaging using a 45° tilted fiber grating," *Opt. Lett.*, vol. 41, no. 11, pp. 2398–2401, 2016.

[30] G. Wang, Z. Yan, L. Yang, L. Zhang, and C. Wang, "Improved resolution optical time stretch imaging based on high efficiency in-fiber diffraction," *Sci. Rep.*, vol. 8, pp. 1–9, 2018.

[31] G. Wang and C. Wang. "Diffraction limited optical time-stretch microscopy using an in-fibre diffraction grating," in *Proc. Front. Opt./Laser Sci.*, 2017, Art. no. FF2A.5.

[32] Z. Yan, C. Mou, K. Zhou, X. Chen, and L. Zhang, "UV-inscription, polarization-dependant loss characteristics and applications of 45° tilted fiber gratings," *J. Lightw. Technol.*, vol. 29, no. 18, pp. 2715–2724, Sep. 2011.

[33] G. Pu, L. Yi, L. Zhang, C. Luo, Z. Li, and W. Hu, "Intelligent control of mode-locked femtosecond pulses by time-stretch-assisted real-time spectral analysis," *Light Sci. Appl.*, vol. 9, no. 13, pp. 114–121, 2020.

[34] C. Mou, H. Wang, B. Bale, K. Zhou, L. Zhang, and I. Bennion, "All-fiber passively mode-locked femtosecond laser using a 45°-tilted fiber grating polarization element," *Opt. Exp.*, vol. 18, no. 18, pp. 18906–18911, 2010.

[35] X. Liu, C. Liao, Z. Tang, J. Wang, Z. Wei, and S. Liu, "Polarization coding and decoding by phase modulation in polarizing sagnac interferometers," in *Proc. SPIE 6827 Quantum Opt., Opt. Data Storage, Adv. Microlithogr.*, 2007, Art. no. 68270I.

[36] E. Compain and B. Drevillon. "High-frequency modulation of the four states of polarization of light with a single phase modulator," *Rev. Sci. Instruments*, vol. 69, pp. 1574–1580, 1998.

[37] J. A. Tropp, J. N. Laska, M. F. Duarte, J. K. Romberg, and R. G. Baraniuk, "Beyond Nyquist: Efficient sampling of bandlimited signals," *IEEE Trans. Inf. Theory*, vol. 56, no. 1, pp. 520–544, Jan. 2010.

[38] E. J. Candes and T. Tao, "Decoding by linear programming," *IEEE Trans. Inf. Theory*, vol. 51, no. 12, pp. 4203–4215, Dec. 2005.

[39] S. Xiao and A. W. Weiner, "An eight-channel hyperfine wavelength demultiplexer using a virtually imaged phased-array (VIPA)," *IEEE Photon. Technol. Lett.*, vol. 17, no. 12, pp. 372–375, Dec. 2005.